Supplementary Information for:

The Amyloid Formation Mechanism in Human IAPP: Dimers have β-strand Monomer-Monomer Interfaces

Author Affiliation:

Nicholas F. Dupuis, Chun Wu, Joan-Emma Shea, and Michael T. Bowers*

Department of Chemistry and Biochemistry, University of California Santa Barbara, Santa Barbara, CA 93106

Experimental Methods:

Peptide Sample Preparation

All samples of human IAPP and rat IAPP were purchased from Bachem (Torrance, CA) or were synthesized in the Raleigh Lab (SUNY Stony Brook) using standard FMOC chemistry.[1] Each sample was dissolved in 100% hexafluoroisopropanol (HFIP) purchased from Sigma (St. Louis) at a concentration of 1mM. Aliquots of the stock were dried and the peptides were re-suspended in 100 mM ammonium acetate buffer at pH 7.0 for final peptide concentrations of 20 μM.

DC Ion Mobility Experiments

All IMS/MS experiments were carried out on a home built instrument. The instrument and operational parameters have been described in detail previously.[2] Briefly, the instrument is organized as follows: nano-electrospray ionization (nano-ESI) source,

ion funnel, drift cell, quadrupole mass analyzer and an electron multiplier detector. All samples were loaded into gold coated borosilicate capillaries that had been pulled to a fine point on a tip puller (Sutter Instrument Co., Novato, CA). The nano-ESI tip is located 1-2 mm in front of a small (0.010" id) orifice leading into the vacuum. A positive voltage was applied to the tip and ions were extracted and enter the instrument where they are collected and focused in the ion funnel. A 10 μs pulse of ions was injected into the drift cell filled with ~5 torr of He gas. They are gently pulled through the buffer gas under the influence of a weak electric field (5-20 V/cm). Following the drift cell the ions were mass analyzed with a quadrupole mass filter and detected with a traditional conversion dynode/electron multiplier arrangement.

After injection into the drift cell, ions experience a constant force from the electric field, *E*. This force is balanced by a retarding frictional force due to collisions with the buffer gas resulting in a constant drift velocity, v_d. The drift velocity is proportional to the magnitude of the electric field and the mobility, *K,* of the ion:

$$\vec{v}_d = K\vec{E} \tag{1}$$

The absolute mobility of an ion is both temperature and pressure dependent so it is customary to report a reduced mobility K_0.

$$K_0 = \left(K \cdot \frac{p}{760} \cdot \frac{273.16}{T} \right) \tag{2}$$

After exiting the drift cell, the ions are mass analyzed and detected as a function of the arrival time, t_A. The reduced mobility can be determined from instrumental parameters by converting equation (1) to equation (3) and plotting t_A versus p/V.

$$t_A = \frac{l^2}{K_0} \cdot \frac{273.16}{760T} \cdot \frac{p}{V} + t_0 \tag{3}$$

In equation 3, l is the length of the drift cell, V is the voltage across the cell, and t_0 is the time the ions spend outside the drift cell before hitting the detector.

It is more intuitive to work with the collision cross section (σ) of an ion and collision theory[3] gives us a relationship of σ to K_0:

$$K_0 = \frac{3q}{16N}\left(\frac{2\pi}{\mu k_b T}\right)^{1/2} \frac{1}{\sigma} \tag{4}$$

In this relationship, N is the buffer gas number density, μ is the reduced mass of the collision system (ion + He) and k_b is Boltzmann's constant. Independent measurements of the collision cross sections are typically reproducible within 1% and are reported as the average of multiple measurements, typically more than three. The reduced mobility (K_0) and subsequently the collision cross section (σ) contain information about the three dimensional configuration of the ion. In the case of peptide ions, secondary and tertiary structural characteristics can be identified by comparison with computational models.

Experimental arrival time distributions can be fit by calculating the flux[3] of ions exiting the drift tube. In this model the ion packet is taken as a periodic delta function and the flux is given by equation 5.

$$\Phi(0,z,t) = \frac{sae^{(-\alpha t)}}{4(\pi D_L t)^{1/2}}\left(v_d + \frac{z}{t}\right)\bullet\left[1 - e^{\left(-r_0^2/4D_T t\right)}\right]e^{\left(-(z-v_d t)^2/4D_L t\right)} \quad (5)$$

Here z is the ion charge, r_0 is the radius of the initial ion packet, a is the area of the exit aperture, D_L and D_T are the longitudinal and transverse diffusion coefficients, s is the initial ion density and α is the loss of ions due to reactions in the drift tube.

The relative contributions of each fitted ATD feature was calculated by integrating the individual Gaussian distributions from the best fit and the contribution reported is the percentage of the total of the fitted ATD.

Human and Rat IAPP Mass Spectra:

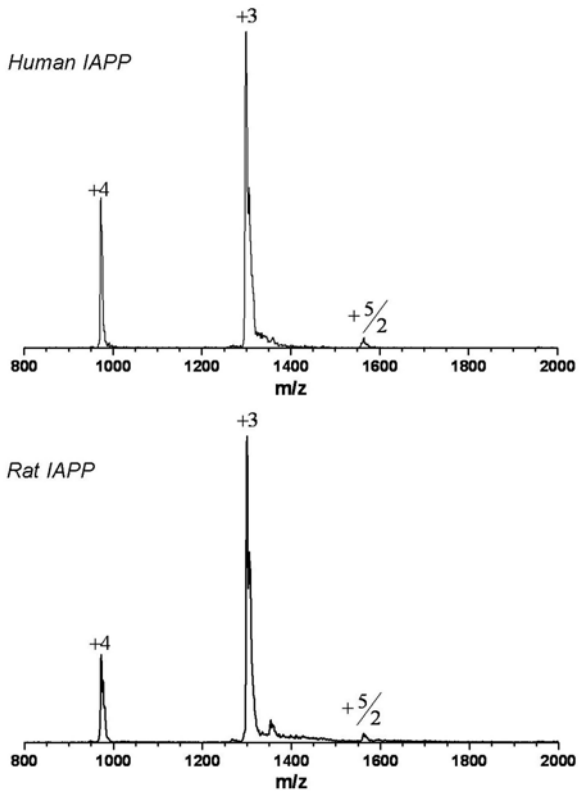

Figure S1. The mass spectra of human (top) and rat (bottom) IAPP were recorded on the homebuilt ion mobility mass spectrometer. The samples were electrosprayed at 20 μM in 100 mM Ammonium Acetate. The two spectra are nearly identical with the z/n = +3 and +4 charge states being most abundant and a small contribution of the z/n = +5/2 dimer.

Molecular Modeling

The AMBER 8[4] simulation package is used in molecular dynamics (MD) simulations. Recent achievements of the AMBER all-atom point-charge protein force field, ff96 with an implicit solvent IGB=5, include the successful ab initio folding of α, β, and α/β proteins and this combination was used to model the peptides in this study.[5-10] Both human and rat IAPP dimerization reactions were modeled in the gas phase and solution. For the hIAPP and rIAPP gas phase trajectories the single most populated gas-phase structural families from our previous studies[5] (Fig. 5 I-J of Ref. 6) were used as the starting structures. These two trajectories are referred to in the text as RGP and HGP for rIAPP and hIAPP respectively. In the solution dimerization the starting monomer conformations for hIAPP and rIAPP were taken from our previous replica exchange molecular dynamics simulations in implicit solvent.[5] rIAPP has two major conformations in solution: helix-coil and coil-rich (Fig. 5 A-B of Ref. 6). From these structures three trajectories were run, two homodimer and one heterodimer. The hIAPP(+3) peptide at neutral pH had three major conformations: helix-loop-hairpin, compact β-sheet rich and extended β-hairpin (Fig. 5 C-E of Ref. 6). In this case six dimerization trajectories were run: three homodimers and three mixed heterodimers. In addition, the β-hairpin homodimer trajectory was run twice, one with anti-parallel orientation and another in a parallel orientation. Thus, seven dimer trajectories were modeled in total for human IAPP(+3). To check the charge effect (H18 is protonated.), we also ran six dimer simulations for hIAPP(+4) at acidic pH based on the three major structural families (Fig. 5 F-H of Ref. 6). In each dimer trajectory the two monomers were started ~40 Å apart in order to model the association of two peptides.

In order to improve sampling efficiency, a harmonic distance restrain is used to keep two monomers close to each other, i.e. when the center-to-center distance is bigger than 60Å, the harmonic force (20 kcal/mol/Å^2) will be applied to the system. Solution phase structures are generated using the recent implicit solvent model (IGB=5)[11] plus the surface term (GBSA=1, 0.005 kcal/Å²/mol) to represent water solvent effects with an effective salt concentration of 0.2 M. For each dimer simulation, an initial energy minimization is performed on the constructed system and the minimized structure is used as the input for a MD simulation of 400 ns. Initial velocities for each system are generated according to the Maxwell-Boltzmann distribution at 300 K. SHAKE[12] is applied to constrain all bonds linking hydrogen atoms and thus a time step of 2.0 fs is used. In order to reduce computation time, non-bonded forces are calculated using a two-stage RESPA (reference system propagator algorithm approach)[13] where the fast varying forces within a 12 Å radius are frequently updated (e.g. every step) and those beyond 12 Å are updated every two steps. The Langevin dynamics is used to control the temperature 300 K using a collision frequency of 1.0 ps^{-1}. The center of mass translation and rotation are removed every 500 MD steps (1.0 ps). The snapshots in the trajectories are saved at 2.0 ps intervals for further analysis.

Selection of Stable Dimer and its Collision Cross Section Calculation

For each dimer system, atom contacts between two monomers (cutoff of 3.0 Å) are calculated to characterize the monomer association. The stable dimers (atom contact is bigger than 20) are formed in some systems. For these stable systems, the last snapshots of the trajectories are used to calculate the binding energy between two

monomers using MM-GBSA (Molecular Mechanics-Generalized Born/Surface Area) module in the AMBER package.[4] Furthermore, the last snapshots of the trajectories are also used to calculate the cross section by a trajectory method.[14, 15] In order to better correlate with the solvent free experiments, these solution phase structures are converted to 'dehydrated' structures via an energy minimization (500000 steps) in vacuum prior to cross section calculations. This "dehydration" reduces the overall size of the structures, while maintaining their solution structural features and in this paper these structures are referred to as "dehydrated solution structures".

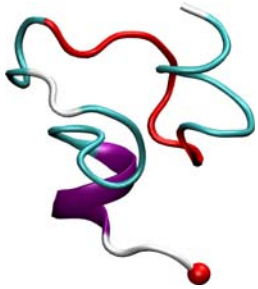	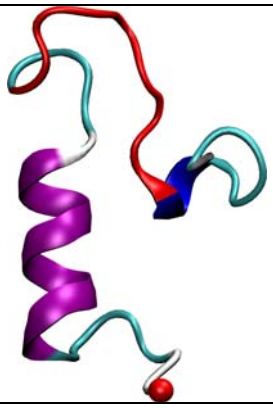		
A	B		I
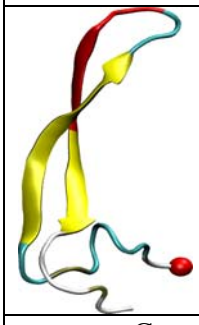	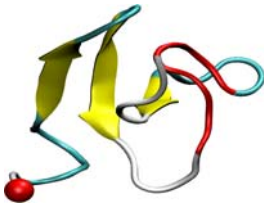	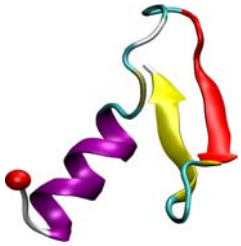	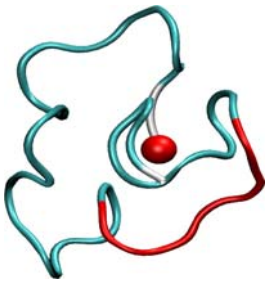
C	D	E	J

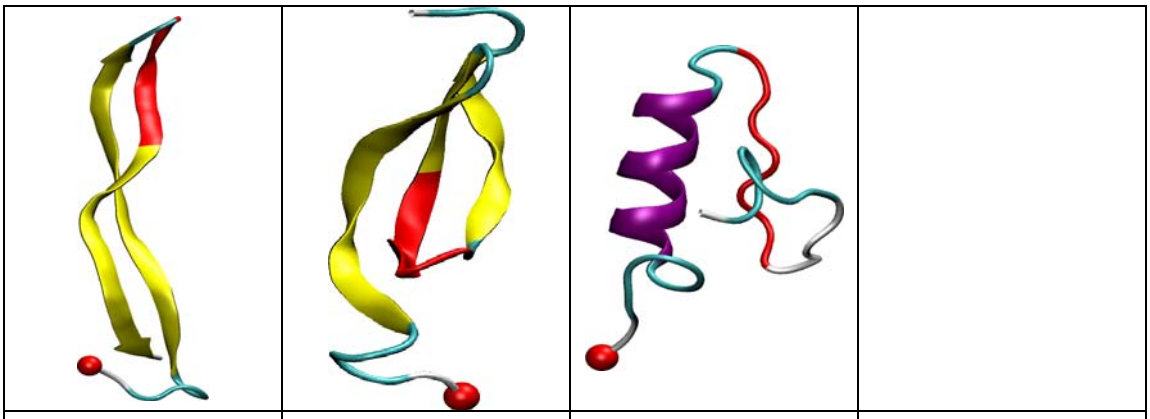

F	G	H	

Figure S2. A summary of the starting structures used in the dimerization simulations. Structures **A** and **B** are the rIAPP solution families, **C**, **D** and **E** are the hIAPP(+3) solution families at neutral pH and **F, G, E** are the IAPP(+4) solution families at acidic pH (i.e. H18 is protonated.). **I** and **J** are the rIAPP and hIAPP(+3) gas phase families respectively. These structures are the most populated structural families identified in the fully equilibrated all-atom REMD simulations performed in our previous study. Residues 22-29 are colored in red. The secondary structure is coded by color: coil in silver, π-helix in pink, 3-10 helix in blue, α-helix in purple, β-sheet in yellow, isolated β-bridge in tan and turn in cyan. N-terminal is shown by a red VDW ball.

Rat IAPP Dimers:

The rat IAPP gas phase trajectory produced a stable dimer which is a compact coil-rich structure.

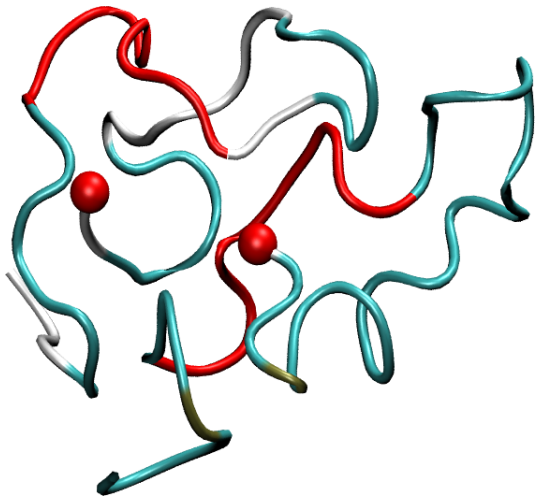

Figure S3. The rIAPP dimer formed in the absence of solvent from two gas phase monomer structures. $\sigma = 1018$ Å^2

The solution rat IAPP dimerization trajectories are shown below. The trajectories plot the number of atomic contacts formed between the two individual peptides. A large number of contacts (> 20) indicate a stable dimer has formed.

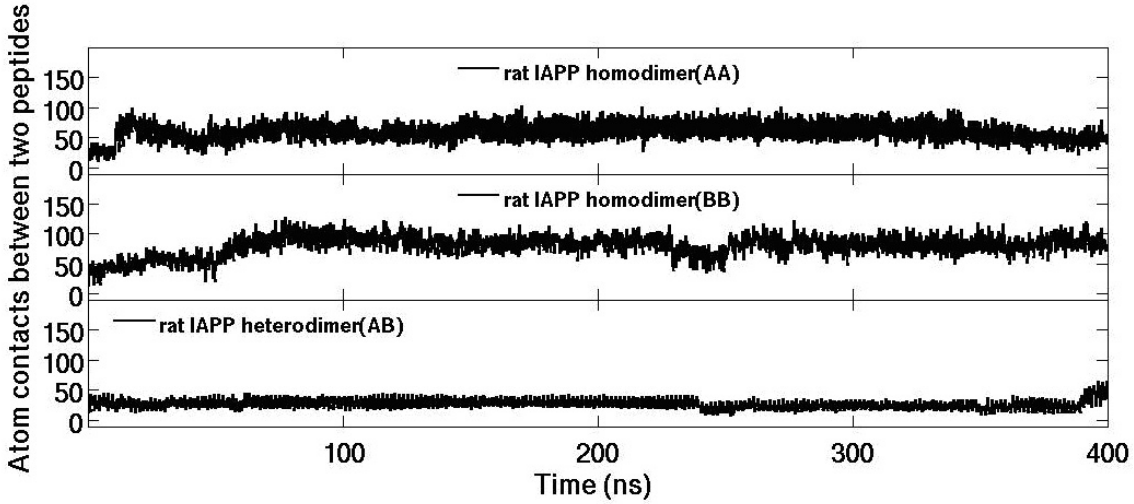

Figure S4. The number of atomic contacts between the two peptide units are shown for each of the three rIAPP dimerization trajectories.

The collision cross section and MM-GBSA binding energy for the formed dimmers are listed together with the structures. The heterodimer formed between the structural families A and B (coil-rich and helix-coil) has strongest binding energy among three dimers.

AA, 1079 Å² -31.2 kcal/mol	AB, 1157 Å² -29.3 kcal/mol	BB, 1116 Å² -54.4 kcal/mol
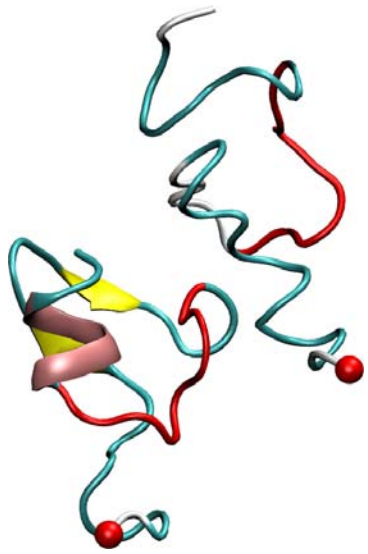	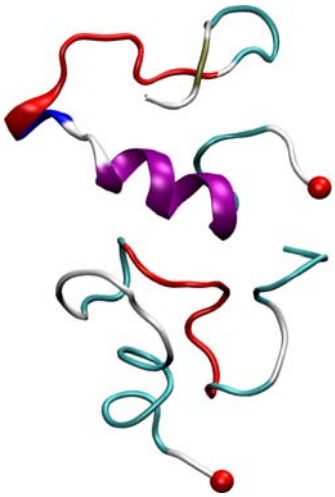	

Figure S5. The snapshots of each of the three solution phase dimerization trajectories. Residues 22-29 are colored in red.

Human IAPP(+3) Dimers under neutral pH conditions:

The structure from the hIAPP gas phase dimerization is shown below.

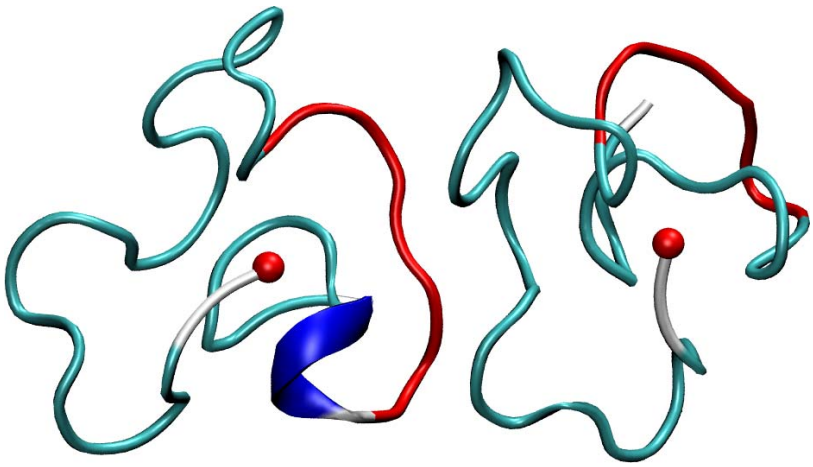

Figure S6. The hIAPP(+4) dimer formed in the absence of solvent from two gas phase monomer structures. $\sigma = 1055$ Å^2

The human IAPP dimerization trajectories for all three major solution families(Fig. 5 C-E of Ref. 6) produced in the REMD simulations in our previous study.[5]

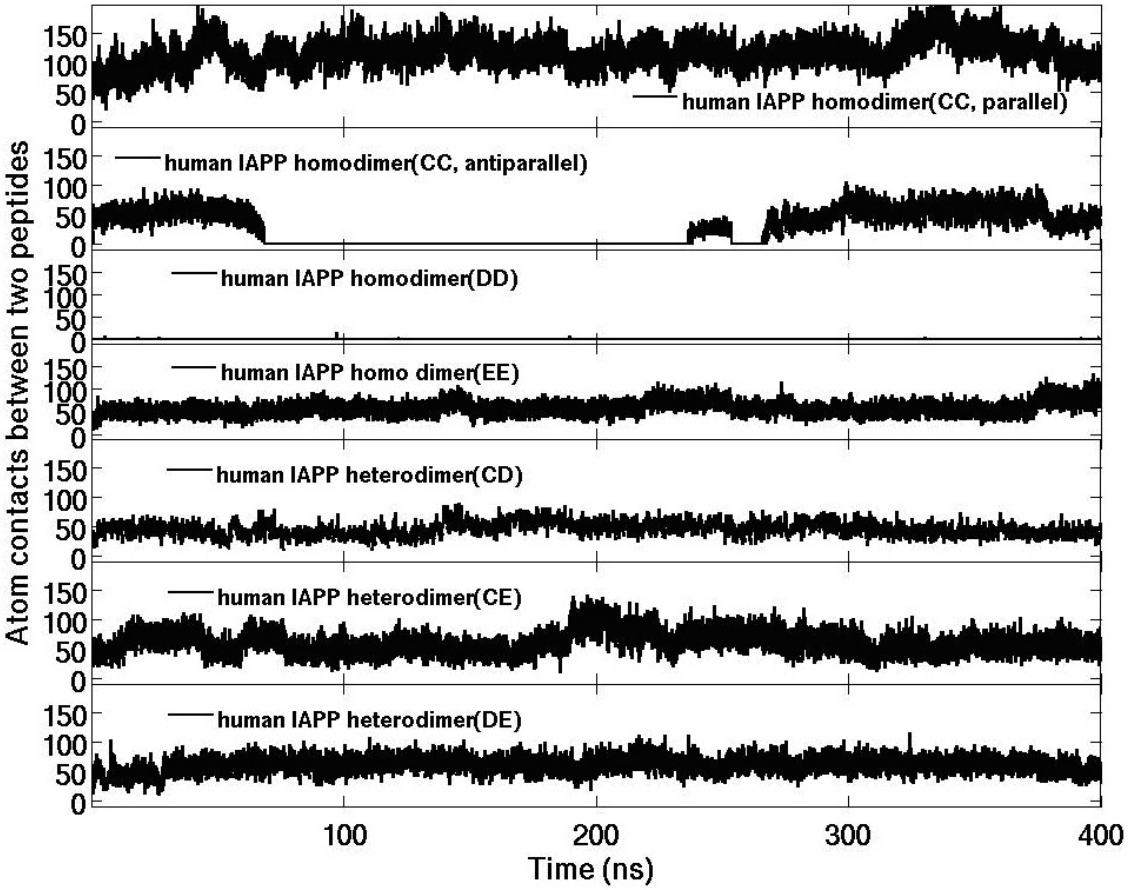

Figure S7. The number of atomic contacts between the two peptide units is shown for each of the seven hIAPP(+3) solution dimerization trajectories.

The structures resulting from the dimerization trajectories of human IAPP(+4) are shown below. There was no dimer formed in the DD trajectory and no structure is shown.

CC parallel, 1150 Å^2 -69.0 kcal/mol	CC anti-parallel, 1352 Å^2 -40.0 kcal/mol	CD, 1035 Å^2 -112.2 kcal/mol
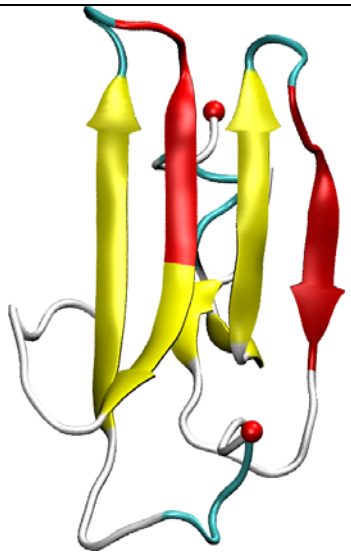	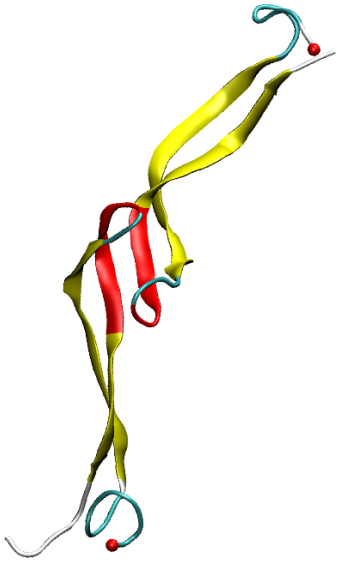	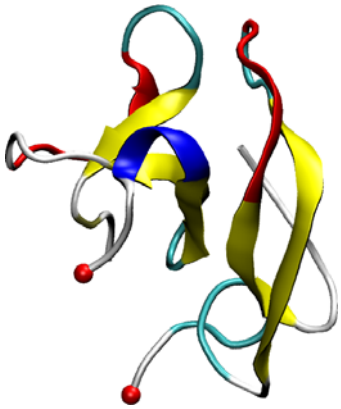
CE, 1172 Å^2 -45.4 kcal/mol	EE, 1105 Å^2 -64.2 kcal/mol	DE, 1118 Å^2 -37.4 kcal/mol
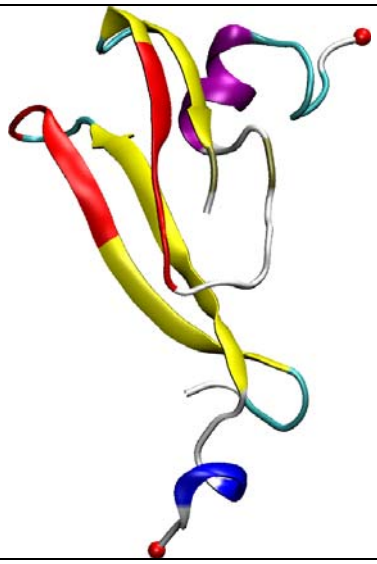	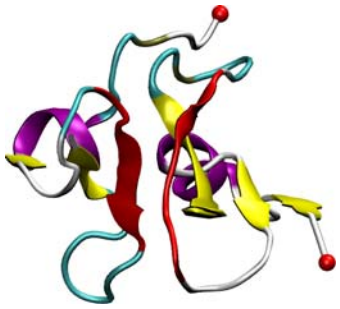	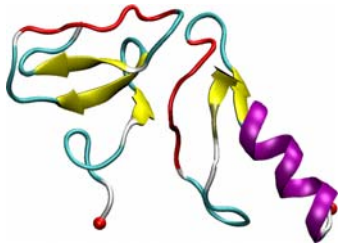

Figure S8. The six structural families from the hIAPP(+3) solution phase dimerization trajectories. No structure is shown for the DD trajectory as no significant contacts were formed during the length of the trajectory. Residues 22-29 are colored in red.

Human IAPP Dimers at acidic condition (i.e. H18 is protonated.):

The human IAPP(+4) dimerization trajectories for all three major solution families(Fig. 5 F-G of Ref. 6) produced in the REMD simulations in our previous study.[5]

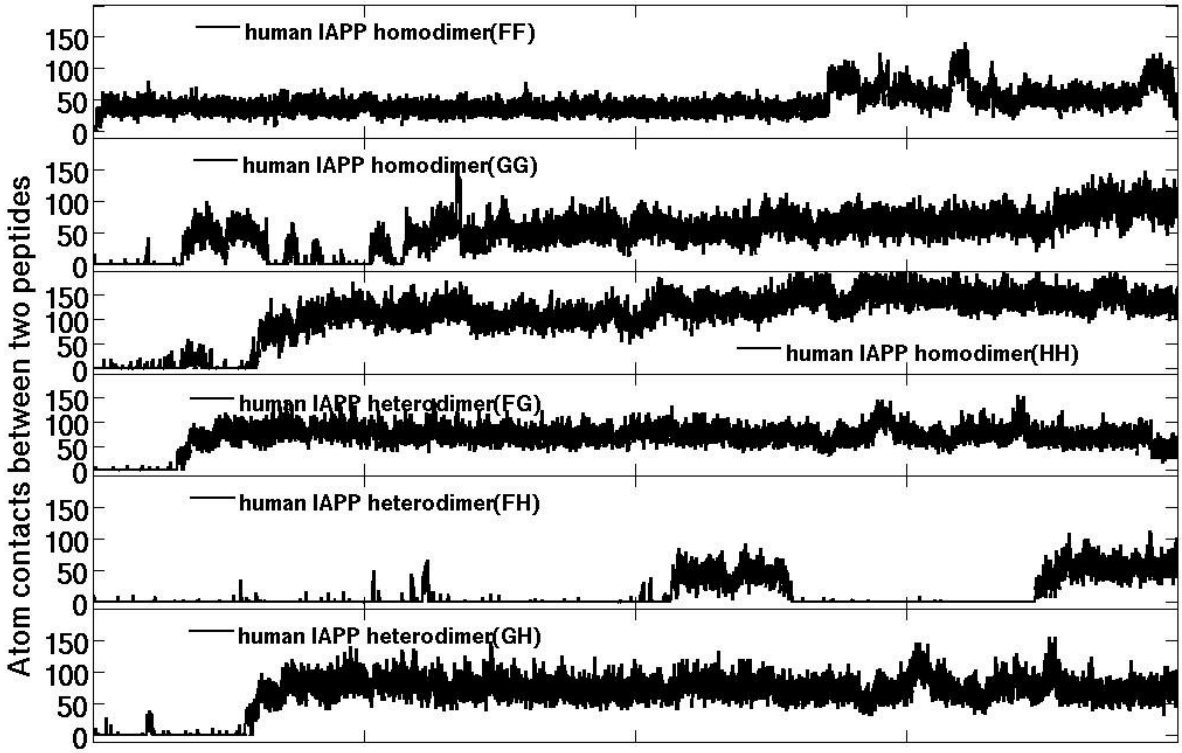

Figure S8. The number of atomic contacts between the two peptide units is shown for each of the six hIAPP(+4) solution dimerization trajectories under acidic condition.

The structures resulting from the dimerization trajectories of human IAPP(+4) are shown below.

FF, 1239Å^2 -75.5 kcal/mol	GG, 1061Å^2 -45.2kcal/mol	HH, 1352Å^2 -115.7 kcal/mol
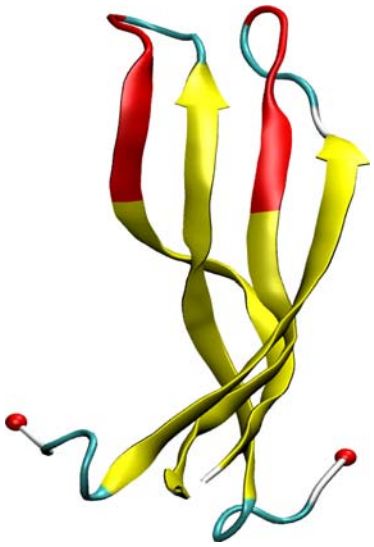		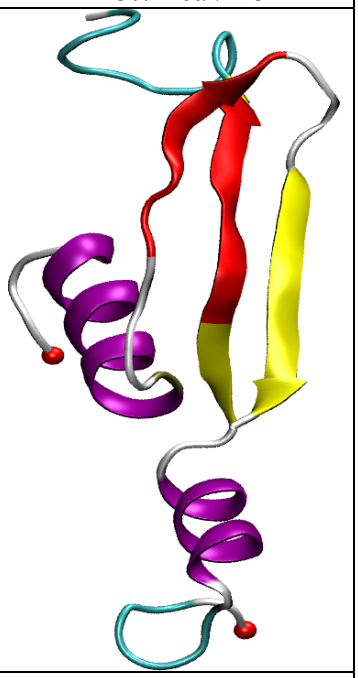
FG, 1247Å^2 -34.4 kcal/mol	FH, 1286Å^2 -50.1 kcal/mol	HG, 1142Å^2 -70.9 kcal/mol
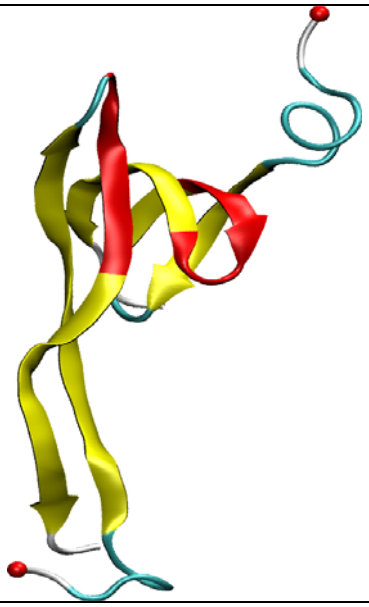	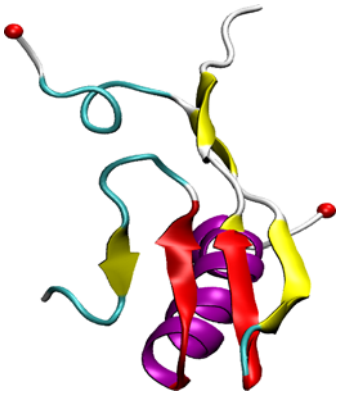	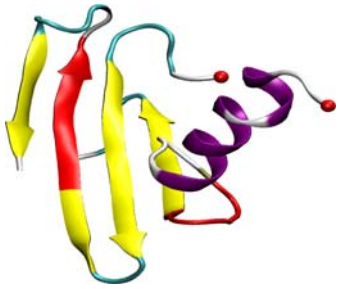

Figure S9. The six structural families from the hIAPP(+4) solution phase dimerization trajectories under acidic condition. Residues 22-29 are colored in red.

References:

(1) Abedini, A.; Singh, G.; Raleigh, D. P., *Anal Biochem* **2006,** *351*, (2), 181-186.
(2) Wyttenbach, T.; Kemper, P. R.; Bowers, M. T., *Int J Mass Spectrom* **2001,** *212*, (1-3), 13-23.
(3) Mason, E. A.; McDaniel, E. W., *Transport properties of ions in gases*. Wiley: New York, 1988; p xvi, 560.
(4) Case, D. A.; Cheatham, T. E.; Darden, T.; Gohlke, H.; Luo, R.; Merz, K. M.; Onufriev, A.; Simmerling, C.; Wang, B.; Woods, R. J., *J Comput Chem* **2005,** *26*, (16), 1668-1688.
(5) Dupuis, N. F.; Wu, C.; Shea, J.-E.; Bowers, M. T., *J Am Chem Soc* **2009,** *131*, (51), 18283-18292.
(6) Shell, M. S.; Ritterson, R.; Dill, K. A., *J Phys Chem B* **2008,** *112*, (22), 6878-6886.
(7) Voelz, V.; Bowman, G.; Beauchamp, K.; Pande, V., *J Am Chem Soc* **2010,** *132*, (5), 1526-+.
(8) Voelz, V.; Singh, V.; Wedemeyer, W.; Lapidus, L.; Pande, V., *J Am Chem Soc* **2010,** *132*, (13), 4702-4709.
(9) Wu, C.; Shea, J.-E., *PLoS Comput Biol* **2010,** *6*, (11), e1000998.
(10) Gunsteren, W. F. v.; Weiner, P. K.; Wilkinson, T., *Computer simulation of biomolecular systems*. Published under the KLUWER/ESCOM imprint by Kluwer Academic Publishers: aordrecht; Boston, 1997; p v.
(11) Onufriev, A.; Bashford, D.; Case, D. A., *Proteins* **2004,** *55*, (2), 383-394.
(12) Ryckaert, J. P.; Ciccotti, G.; Berendsen, H. J. C., *J Comput Phys* **1977,** *23*, (3), 327-341.
(13) Procacci, P.; Berne, B. J., *Mol Phys* **1994,** *83*, (2), 255-272.
(14) Shvartsburg, A. A.; Jarrold, M. F., *Chem Phys Lett* **1996,** *261*, (1-2), 86-91.
(15) Mesleh, M. F.; Hunter, J. M.; Shvartsburg, A. A.; Schatz, G. C.; Jarrold, M. F., *Journal of Physical Chemistry* **1996,** *100*, (40), 16082-16086.